# Trapped modes in waveguides with many small discontinuities

Sergey S. Kurennoy
*Physics Department, University of Maryland, College Park, Maryland 20742*
(Received 22 July 1994)

It has been demonstrated recently [G.V. Stupakov and S.S. Kurennoy, Phys. Rev. E **49**, 794 (1994)] that a single small discontinuity (such as an enlargement or a hole) on a smooth waveguide can result in the appearance of trapped electromagnetic modes with frequencies slightly below the waveguide cutoff frequencies. The present paper studies a similar phenomenon for a waveguide with many small discontinuities, which is a good model for the vacuum chamber of large accelerators. Frequencies of trapped modes and their contributions to the coupling impedance are calculated. The frequencies for the cases of a few discontinuities or a periodic structure coincide well with those from numerical simulations. The trapped modes produce sharp resonance peaks of the coupling impedance near the cutoff frequencies. The magnitude of these peaks, as well as the existence itself of a trapped mode, strongly depends on the distribution of discontinuities, or on the distance between them if a regular array is considered. The impedance in the extreme case can be as large as $N^3$ times that for a single discontinuity, where $N$ is the number of discontinuities.

PACS number(s): 41.75.−i, 41.20.−q

## I. INTRODUCTION

Previous computer studies of cavities coupled to a beam pipe indicated that the impedance of small chamber enlargements exhibits sharp narrow peaks at frequencies close to the cutoff frequencies of the waveguide; see references cited in [1–4]. For the case of a single small discontinuity, such as an enlargement or a hole, on a smooth waveguide it was demonstrated [1] that these peaks can be attributed to trapped modes localized near the discontinuity. The existence of a trapped mode depends on the relation between the conductivity of the chamber walls and a typical size of the discontinuity, and in the limit of perfectly conducting walls the trapped modes exist even for very small perturbations.

This phenomenon can be dangerous for the beam stability in large superconducting proton colliders such as Large Hadron Collider (LHC), where the design anticipates a thermal screen (liner) inside the beam pipe [5]. The function of the liner is to screen the cold walls of the vacuum chamber from synchrotron radiation in order to prevent wall heating and photodesorption of molecules stuck to the cold wall. The liner walls contain many small pumping holes, which work as a distributed cryopump to provide high vacuum in the beam region, and have an inner copper coating to slow down the resistive wall instability. In such a structure with many small discontinuities and very high wall conductivity at cryogenic temperatures, the trapped modes can exist and contribute significantly to the beam-chamber coupling impedances.

The trapped modes in a waveguide with many discontinuities are considered in the present paper. In Sec. II we present some results for the trapped modes produced by a single small discontinuity. Section III is devoted to the case of a finite number of discontinuities and Sec. IV deals with periodic arrays. Estimates of the coupling impedance near the cutoff frequency for liners are given in Sec. V.

## II. A SINGLE DISCONTINUITY

Let us consider a cylindrical waveguide with perfectly conducting walls having a small axisymmetric enlargement, so that a characteristic dimension of this discontinuity is much smaller than the pipe radius $b$. It was shown [1] that there is a solution of the Maxwell equations for this structure with the frequency $\Omega_1$ slightly below the cutoff frequency $\omega_1 = \mu_1 c/b$, where $\mu_m$ is the $m$th root of the Bessel function $J_0$, $m = 1, 2, \ldots$. Far from the discontinuity (in fact, at distances $|z| > b$) the fields of the TM trapped mode have the form

$$\begin{aligned} \mathcal{E}_z^{(1)} &= \frac{\mu_1^2}{b^2} J_0\left(\frac{\mu_1 r}{b}\right) \exp(-k_1|z|) \,, \\ \mathcal{E}_r^{(1)} &= \mathrm{sgn}(z) \frac{\mu_1 k_1}{b} J_1\left(\frac{\mu_1 r}{b}\right) \exp(-k_1|z|) \,, \\ Z_0 \mathcal{H}_\theta^{(1)} &= -\frac{i\omega\mu_1}{cb} J_1\left(\frac{\mu_1 r}{b}\right) \exp(-k_1|z|) \,, \end{aligned} \tag{1}$$

where $Z_0 = \sqrt{\mu_0/\varepsilon_0} = 120\pi\ \Omega$, and the propagation constant $k_1 = \sqrt{\omega_1^2 - \Omega_1^2}/c$ is given by

$$k_1 = \frac{\mu_1^2 A}{b^3} \,, \tag{2}$$

where $A$ is the area of the cross section of the enlargement in the $rz$ plane. (It was derived using the Lorentz reciprocity theorem. In fact, the same can be done in other ways, for example, from the equality $\varepsilon_0 \int |\mathcal{E}|^2 dV = \mu_0 \int |\mathcal{H}|^2 dV$, which is just energy conservation [6].) Note that $A$ enters Eq. (2) with its sign; e.g., for an iris that

 

protrudes into the pipe, $A$ would have a negative sign and solution (1) would not exist. We assume from the beginning that $k_1 b \ll 1$ or, in words, the trapped mode is spread along the axis of the pipe over the distance $l_1 \equiv k_1^{-1}$ much longer than the waveguide radius, i.e., $l_1 \gg b$.

For the frequency shift $\Delta\omega_1 = \omega_1 - \Omega_1$ we get

$$\Delta\omega_1 = \omega_1 \frac{\mu_1^2}{2} \left(\frac{A}{b^2}\right)^2 . \tag{3}$$

For the case of a finite, though large, conductivity of the walls, as a result of energy dissipation in the walls, the trapped mode frequency acquires a negative imaginary part $\Omega_1 \to \Omega_1 - i\gamma_1$. The damping rate $\gamma_1$ is

$$\gamma_1 = \frac{\omega_1 \delta}{2b} , \tag{4}$$

where $\delta = \sqrt{2/(\mu_0 \sigma \omega_1)}$ is the skin depth in the pipe wall whose conductivity is $\sigma$. The trapped mode disappears when $\gamma_1$ becomes larger than $\Delta\omega_1$.

The longitudinal impedance produced by the trapped mode is calculated as that for a cavity with given eigenmodes (see [4]):

$$Z_1(\omega) = \frac{2i\Omega_1 \gamma_1 R_1}{\omega^2 - (\Omega_1 - i\gamma_1)^2} , \tag{5}$$

where the shunt impedance $R_1$ is

$$R_1 = \frac{Z_0 \mu_1^3 A^3}{\pi \delta b^5} . \tag{6}$$

In the limit of perfect conductivity, $\delta \to 0$, Eq. (5) gives an infinitely high and narrow peak. Expression (6) is different from that obtained in [1], namely,

$$R_1 = \frac{4 Z_0 \mu_1 A^3}{\pi \delta b^5 J_1^2(\mu_1)} ,$$

since Eq. (6) includes contributions from higher-order waveguide modes. While amplitudes of excitation of higher modes are small (they are calculated using the approach of Ref. [7]), their sum contribution to the impedance is comparable to that of the lowest mode given by Eqs. (1) because $R_1$ happens to be sensitive to the field shape near the discontinuity [8]. One should recall that the trapped mode is described by Eqs. (1) only far from the discontinuity, $|z| > b$, but for shorter distances the field is formed also by many evanescent waveguide modes.

It was shown that a small hole in the pipe wall also creates localized axisymmetric trapped modes [1]. All the results for an enlargement remain valid for the hole if we put the quantity $\alpha_\theta/(4\pi b)$, where $\alpha_\theta$ is the magnetic susceptibility of the hole, in Eqs. (2)–(6) instead of the area $A$ of the enlargement cross section:

$$A \to \frac{\alpha_\theta}{4\pi b} . \tag{7}$$

A similar study has been performed for higher-order and TE waveguide modes and the existence of trapped modes in these cases was also demonstrated [1].

One can calculate the transverse impedance due to trapped modes in a similar way. The lowest transverse resonance occurs near the cutoff frequency $\omega_{11} = \mu_{11} c/b$ of the $TM_{11}$ mode, where $\mu_{1m}$ is the $m$th root of the Bessel function $J_1$. The resonance impedance has a form

$$\vec{Z}_{\perp 1}(\omega) = \frac{2i\Omega_{11}\gamma_{11} R_{\perp 1}}{\omega^2 - (\Omega_{11} - i\gamma_{11})^2} \hat{\vec{a}}_b , \tag{8}$$

where for a symmetric enlargement the frequency shift $\Delta\omega_{11} = \omega_{11} - \Omega_{11}$ and damping rate $\gamma_{11}$ are given by Eqs. (3) and (4) with $\mu_1$ replaced by $\mu_{11}$, $\hat{\vec{a}}_b$ is a unit vector in the direction of the beam transverse offset in the transverse chamber cross section where the discontinuity is located, and the shunt transverse impedance is

$$R_{\perp 1} = \frac{Z_0 \mu_{11}^4 A^3}{2\pi \delta b^6} . \tag{9}$$

This expression again includes contributions from higher modes and replaces the result

$$R_{\perp 1} = \frac{4 Z_0 \mu_{11}^2 A^3}{\pi \delta b^6 J_0^2(\mu_{11})} ,$$

which would take place if only the lowest mode is taken into account.

In the case of a hole the structure loses its symmetry, and in Eq. (8) the vector $\hat{\vec{a}}_b$ should be replaced by $\hat{\vec{a}}_h \cos(\theta_b - \theta_h)$, where $\hat{\vec{a}}_h$ is a unit vector in the direction to the hole and $\theta_b, \theta_h$ are the azimuthal angles of the beam and hole, respectively, in the cross section plane; see Ref. [7]. It means that the deflecting force is directed to (or opposite) the hole and its magnitude depends on the angle between the beam-offset vector and the direction to the hole. As for the value of $R_{\perp 1}$, one should substitute $\alpha_\theta/(2\pi b)$ instead of $A$ in Eq. (9).

## III. MANY DISCONTINUITIES

Consider an axisymmetric waveguide with $N$ small enlargements located at $z_1, z_2, \ldots, z_N$ and having areas $A_1, A_2, \ldots, A_N$ of the longitudinal cross section, respectively. In this structure, we will look for a solution of the Maxwell equations with a frequency $\Omega$ slightly below the cutoff frequency $\omega_1$. Let us introduce the propagation constant $k = \sqrt{\omega_1^2 - \Omega^2}/c$ and consider the following piecewise form of the solution [only $z$ dependence is shown below; the radial behavior corresponds to Eq. (1) for $\mathcal{E}_z$, $\mathcal{E}_z$, and $\mathcal{H}_\theta$, respectively]:

$$a_1 \exp(kz) \qquad \text{for} \quad z < z_1 ,$$

$$a_{n+1} \exp(kz) + b_n \exp(-kz)$$

$$\text{for} \quad z_n < z < z_{n+1} , \; n = 1, 2, \ldots, N-1 , \tag{10}$$

$$b_N \exp(-kz) \qquad \text{for} \quad z > z_N ,$$

where $a_i, b_i$, $n = 1, 2, \ldots, N$, are amplitudes to be determined. We assume here, as well as in the case of a single discontinuity, that $kb \ll 1$ and the form of the solution above is justified when enlargements are spaced at least by the distance of the order of the chamber diameter, so that one can neglect higher modes which are essential only very close to discontinuities, namely, at distances a few times smaller than the chamber radius.

To find the eigenfrequency of the trapped mode we use continuity conditions and the Lorentz reciprocity theorem. It states that for any two solutions of Maxwell's equations without sources the following equality holds [9]:

$$\int dS\vec{n}(\vec{E}_1 \times \vec{H}_2 - \vec{E}_2 \times \vec{H}_1) = 0 \ , \tag{11}$$

where the integration runs over a closed surface $S$ consisting of the surface of the waveguide wall and two plane end surfaces which are transverse to the waveguide axis. We take $\vec{E}_1 = \vec{\mathcal{E}}$, $\vec{H}_1 = \vec{\mathcal{H}}$ and choose $\vec{E}_2, \vec{H}_2$ to be a TM mode having frequency $\Omega$, the same as the trapped mode, and exponentially decaying either as $\exp(-kz)$ in the positive direction or as $\exp(kz)$ in the negative one. Due to the orthogonality of the radial eigenfunctions the only contribution to the end-surface integrals comes from terms with factor $\exp(kz)$ [or $\exp(-kz)$] opposite that of the chosen TM mode. The only contribution to the wall integral comes from the regions of the waveguide enlargements; see [1] for more detail. We choose the positions of the end surfaces in such a way that the wall integration in Eq. (11) includes only one discontinuity at a time and apply this procedure twice to all discontinuities in turn using first the TM mode with $\exp(-kz)$ behavior and then the TM mode with $\exp(kz)$. In fact, for the first and the last enlargements, which belong to the semi-infinite intervals, we use the integration with only one of the two possible TM modes. One more equation for each of these two discontinuities follows from the field continuity:

$$\begin{aligned} &a_1 \exp(kz_1) = b_1 \exp(-kz_1) + a_2 \exp(kz_1) \ , \\ &b_{N-1} \exp(-kz_N) + a_N \exp(kz_N) = b_N \exp(-kz_N) \ . \end{aligned} \tag{12}$$

Other $2N-2$ equations follow from the reciprocity as described above:

$$\begin{aligned} &-a_1 + y_1 a_1 + a_2 = 0 \ , \\ &-a_n + y_n \left[a_n + b_{n-1} \exp(-2kz_n)\right] + a_{n+1} = 0 \\ &\qquad\qquad n = 2, \ldots, N-1 \\ &-b_n + y_n \left[b_n + a_{n+1} \exp(2kz_n)\right] + b_{n-1} = 0 \ , \\ &\qquad\qquad n = 2, \ldots, N-1 \\ &-b_N + y_N b_N + b_{N-1} = 0 \ , \end{aligned} \tag{13}$$

where the following notations are introduced: $y_n = d_n/x$, $d_n = \mu_1^2 A_n/b^2$, and $x = kb$. Combining (13) and (12) we get $2N$ simultaneous homogeneous equations for $2N+1$ variables: amplitudes $a_i, b_i$ and propagation constant $k$. The condition for the solutions for $a_i, b_i$ to exist, i.e., the determinant of the matrix on the left-hand side (LHS) of the equations above to vanish, gives us an equation for the propagation constant and hence for the frequency of the trapped mode.

Due to the structure of the matrix, which has three or fewer nonzero elements in each column or row, this equation can be written recurrently for any given number $N$ in terms of all the LHS of the equations for lower numbers of discontinuities. In the notations introduced above, Eq. (2) for $N = 1$ can be rewritten as

$$1 - y = 0 \ ,$$

where $y = d/x$ with $d = \mu_1^2 A/b^2$ and $x = kb$. The small parameter $d$ is just the ratio of the waveguide radius $b$ to the length $l_1$ of the region occupied by the fields of the trapped mode for a single discontinuity; cf. Eq. (2). For the case $N = 2$ from (13) and (12) we get

$$D_{1,2}(k) \equiv (1 - y_1)(1 - y_2) - \exp(-2kg_{1,2}) y_1 y_2 = 0 \ , \tag{14}$$

where $g_{i,k} = z_k - z_i$ $(k > i)$ is a longitudinal spacing between the $i$th and $k$th discontinuities. Similarly, for $N = 3$ the equation is

$$D_{1,3}(k) \equiv D_{1,2}(k) D_{2,3}(k) - \exp(-2kg_{1,3}) y_1 y_3 = 0 \ . \tag{15}$$

For the case of $N > 3$ discontinuities the equation can be written in the form

$$\begin{aligned} D_{1,N}(k) \equiv\ & D_{1,N-1}(k) D_{N-1,N}(k) \\ & - \sum_{m=2}^{N-2} D_{1,m}(k) \exp(-2kg_{m,N}) y_m y_N \\ & - \exp(-2kg_{1,N}) y_1 y_N = 0 \ , \end{aligned} \tag{16}$$

which can be proved by induction. Multiplying by $k^{2N-2}$ the LHS of the equation, one can reduce it to a polynomial of the power $(2N-2)$ in $k$, except for the exponential dependence on $k$ in its coefficients.

### A. $N = 2$

To study the frequencies of trapped modes in the system of two discontinuities, it is convenient to introduce the following: the ratio of areas of two enlargements $\rho = A_2/A_1 > 1$; $d = \mu_1^2 A_1/b^2$; the variable $u = x/d$ is the ratio of the propagation constant $k$ for a $N = 2$ trapped mode to that in the case of a single discontinuity $k_1$, given by Eq. (2) with $A = A_1$; and the parameter $r = gd/b = g/l_1$ is the ratio of the distance between discontinuities to the length $l_1$ of the region occupied by the trapped mode for a single discontinuity with area $A_1$,

i.e., $l_1 = b/d = b^3/(\mu_1^2 A_1)$; cf. Eq. (2). In these notations, Eq. (14) takes the form

$$(u-1)(u-\rho) - \rho \exp(-2ur) = 0 \ . \qquad (17)$$

We are interested only in positive solutions of this equation. Factorizing it as product of two "linear" equations

$$\left[2u - \rho - 1 - \sqrt{(\rho-1)^2 + 4\rho\exp(-2ur)}\right]$$

$$\times \left[2u - \rho - 1 + \sqrt{(\rho-1)^2 + 4\rho\exp(-2ur)}\right] = 0 \ , \qquad (18)$$

one can easily find out that there are two positive solutions. The first one $u_s$ exists for any positive value of parameter $r$ and decreases asymptotically in the range from $\rho + 1$ at small $r$ to $\rho$ when $r \gg 1/\rho$. The second solution $u_a$ exists only for $r > (\rho+1)/(2\rho)$ and increases asymptotically from 0 to 1 with an increase in $r$ (see Fig. 1 for $\rho = 2$). The asymptotic values $\rho$ and 1 obviously correspond to the two independent trapped modes for the two discontinuities separated so far that they do not "feel" each other, and each mode is described separately by Eq. (2).

The case of two identical discontinuities $\rho = 1$ is very interesting. The factorized Eq. (18) is especially simple in this case:

$$[u - 1 - \exp(-ur)]\,[u - 1 + \exp(-ur)] = 0 \qquad (19)$$

and both its solutions tend to 1 at large $r$. The physical interpretation of the two possible solution can be easily found from Eqs. (12) and (13): $u_s$ gives a symmetric field and $u_a$ an antisymmetric one, i.e., the fields are zero in the midpoint between the two identical enlargements for the second solution. The antisymmetric solution exists only for large spacings (see Fig. 2) and its frequency shift is always smaller than that for a single discontinuity with the same area. It should be noted here that frequency shifts are assumed to be small compared to the cutoff frequency and they are approximately proportional to $u^2$; cf. Eq. (3).

The behavior of the symmetric solution $u_s$ at small $r$ is also easy to explain: when two enlargements are very close to each other they work like a single enlargement with area $A = A_1 + A_2$. It corresponds to the limit

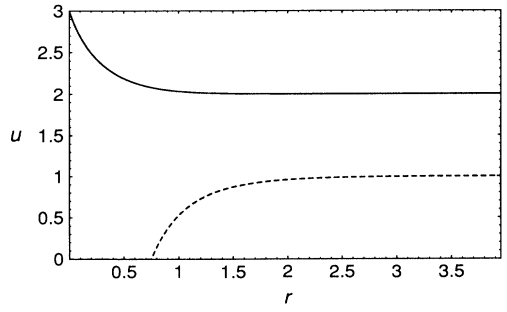


FIG. 1. Ratio $u = k/k_1$ versus $r = g/l_1$ for two discontinuities with $\rho = 2$.

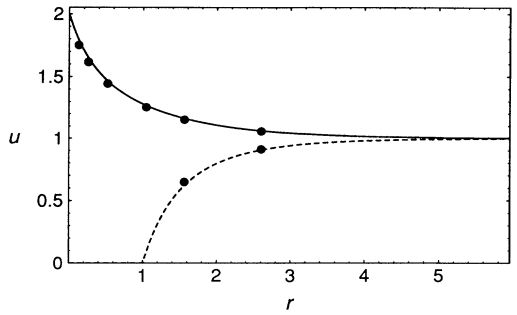


FIG. 2. Ratio $u = k/k_1$ versus $r$ for symmetric (solid line) and antisymmetric (dashed line) modes. Thick points show numerical results.

$u_s \to \rho + 1$ in the general case of two discontinuities (and $u_s \to 2$ for two identical ones) when $r \to 0$.

It is appropriate to mention an obvious analogy of the problem under consideration with the well-known problem of two narrow potential wells in quantum mechanics. To check our analytical results for frequencies, we have carried out numerical computations of the lowest eigenfrequencies in a long cylindrical resonator with two small pill boxes by means of the computer code SUPERFISH [10] varying the distance between the pillboxes. The waveguide cutoff frequency $\omega_1$ corresponds to the eigenfrequency of the $E_{010}$ mode in the smooth (without pill boxes) resonator with the same radius, but the presence of enlargements shifts the eigenfrequency down. To exclude the influence of the sidewalls, one has to choose the length $L$ of the resonator to be larger than the region where the trapped mode is localized, $L \gg l_1 = b^3/(\mu_1^2 A)$. We have used $b = 2$ cm, $A_1 = A_2 = A = 0.18$ cm$^2$ ($d = 0.26$), $g$ =1–20 cm, and $L$ from 40 cm to 100 cm. Figure 2 shows that numerical and analytical results are in good agreement. Figures 3 and 4 show the electric field lines for resonator eigenmodes that correspond to the symmetric and antisymmetric trapped modes in the waveguide with two enlargements (only one-quarter of the longitudinal cross section of the resonator is shown).

The resonant contributions of trapped modes to the beam-chamber coupling impedance can be calculated in the same way as in the case of a cavity with known eigenmodes; see Ref. [4] for details. The peak value of the longitudinal impedance in the resonance can be evaluated as

$$R_2 = \frac{\sigma\delta\left|\int dz \exp(-i\Omega z/c)\mathcal{E}_z(z)\right|^2}{\int_S ds|\mathcal{H}_\tau|^2} \ , \qquad (20)$$

where $\mathcal{H}_\tau$ is the tangential component of the magnetic field near the wall, integration in denominator is performed over the inner waveguide surface, $\sigma$ is conductivity of the pipe wall, and $\delta = \sqrt{2/(\mu_0\sigma\omega_1)}$ is the skin depth. Performing the integration and taking into account that the frequency $\Omega$ of the trapped mode is very close to the cutoff frequency $\omega_1 = \mu_1 c/b$ leads to the expression

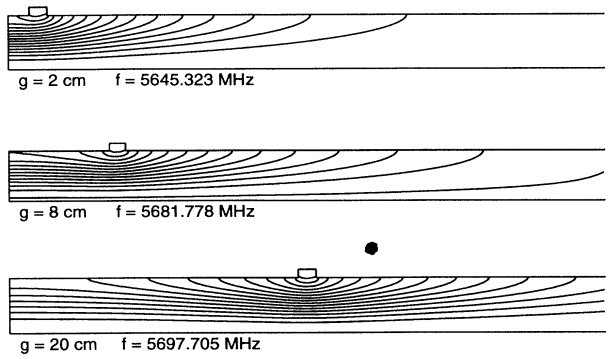


FIG. 3. Electric field lines in symmetric trapped modes.

$$R_2 = R_1 u^3 \frac{u(1+\rho) + 2\rho\,[\exp(-ur)\cos(\mu_1 g/b) - 1]}{u(1+\rho) + 2\rho\,[\exp(-2ur)(1+ur) - 1]}\ , \tag{21}$$

where $R_1 = (Z_0\mu_1^3 A_1^3)/(\pi\delta b^5)$ is just the impedance for a single enlargement with area $A_1$ [cf. Eq. (6)], and $u = u(r,\rho)$ is a solution of Eq. (17).

The extreme cases of small ($r \to 0$) or large ($r \gg 1$) distances between discontinuities can be derived easily basing on the study of Eq. (17) above. For small $r$ the ratio of impedances of two discontinuities to the impedance of the smallest one of them, $R_2/R_1$, tends to $(1+\rho)^3$ for the "symmetric" solution $u_s$. For large distances, $R_2/R_1$ becomes $\rho^3$ for $u_s$ and 1 for $u_a$. There are some oscillations at intermediate distances; see Fig. 5.

Expression (21) takes an even more simple form for the case of two identical discontinuities $\rho = 1$:

$$R_2 = R_1 \frac{u^3\,[1 \pm \cos(\mu_1 g/b)]}{1 \pm \exp(-ur)(1+ur)}\ , \tag{22}$$

where the upper sign corresponds to the symmetric solution $u = u_s(r)$, which satisfies $u - 1 - \exp(-ur) = 0$, and the lower one to the antisymmetric solution $u = u_a(r)$, which satisfies $u - 1 + \exp(-ur) = 0$. The asymptotic behavior of (22) at large distances can be found using asymptotics $u_s \to 1 + e^{-r}$ and $u_a \to 1 - e^{-r}$. The ratio $R_2/R_1$ becomes $[1 \pm \cos(\mu_1 g/b)]$. While the sum of these impedances is just twice the impedance of a single enlargement, there are strong oscillations for each of two modes. The ratio $R_2/R_1$ is plotted in Fig. 5 for $\rho = 2$ and in Fig. 6 for $\rho = 1$.

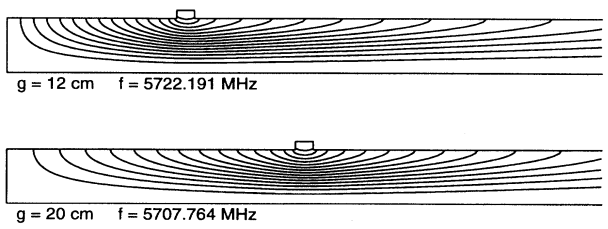


FIG. 4. Electric field lines in antisymmetric trapped modes.

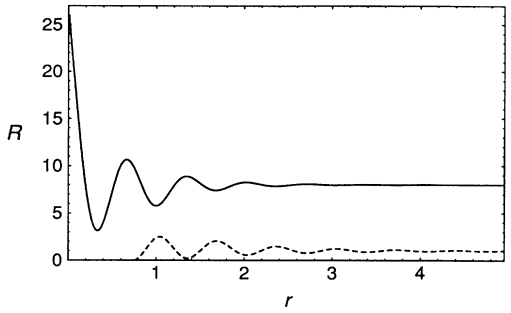


FIG. 5. Impedance ratio $R = R_2/R_1$ versus $r = g/l_1$ for two discontinuities with $\rho = 2$ (parameter $d = 0.26$).

### B. $N$=3

We restrict ourselves here only to the case of three identical equidistant discontinuities, i.e., $d_i = d$, $i = 1,2,3$, and $g_{1,2} = g_{2,3} = g$. Equation (15) transforms into the factorized equation

$$(u-1)[u - 1 + \exp(-2ur)]$$

$$\times\,[(u-1)^2 - (u+1)\exp(-2ur)] = 0\ , \tag{23}$$

where again $u = kb/d = k/k_1$ and $r = gd/b = g/l_1$. One can easily recognize that the expression in the second brackets gives an antisymmetric trapped mode for two enlargements spaced by $2g$ [compare Eq. (19)] and the enlargement in the middle just does not play a role in this case since the trapped mode fields vanish near its location. The first brackets gives an extraneous root, while the "quadratic" equation in the square brackets has two positive solutions which correspond to symmetric trapped modes. The first solution $u_{s0}$, corresponding to fields without nodes, exists for all positive values of $r$ and tends to 3 at small $r$. The second one $u_{s1}$ exists only when $r > 3/2$ and gives a trapped mode with two

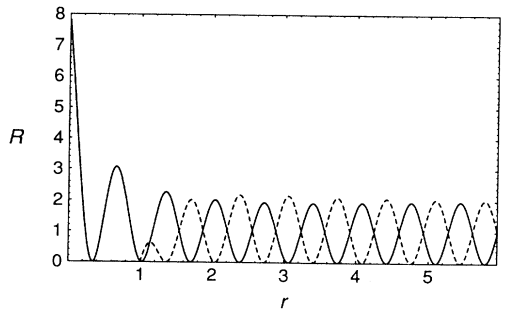


FIG. 6. Impedance ratio $R$ versus $r$ for two identical discontinuities ($d = 0.26$). The solid line is for the symmetric mode, the dashed line for the antisymmetric mode.

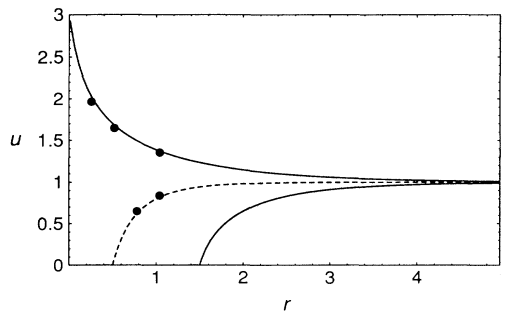


FIG. 7. Ratio $u = k/k_1$ versus $r = g/l_1$ for three identical discontinuities. Solid lines are for symmetric modes, the dashed line is for the antisymmetric mode. Thick points show numerical results.

nodes. All three solutions go asymptotically to 1 at large distances between discontinuities. Figure 7 shows the three solutions of Eq. (23) versus the spacing between discontinuities, as well as comparison with results of some numerical computations using SUPERFISH.

The impedance for the antisymmetric trapped mode is given by Eq. (22) with the minus sign and $g \to 2g$, $r \to 2r$ substituted. For the symmetric modes one can obtain

$$R_3 = R_1 u \frac{[\exp(ur)(u-1) + \exp(-ur) + 2u\cos(\mu_1 g/b)]^2}{3u + 1 - \exp(-2ur) + 4ur(u-1)} . \tag{24}$$

The derivation and notations used are similar to those of Eq. (21). At small distances, the ratio $R_3/R_1$ for the maximal symmetric mode $u_{s0}$ goes to $3^3 = 27$ and at large distances it oscillates as $[1+\sqrt{2}\cos(\mu_1 g/b)]^2/2$. The second symmetric mode exhibits similar oscillations $[1 - \sqrt{2}\cos(\mu_1 g/b)]^2/2$ at large $r$. The impedance versus the distance between discontinuities is plotted in Fig. 8. In spite of the oscillations for each of the trapped modes, the sum of the impedances for all three modes becomes triple that for a single discontinuity at large spacings in which case all three modes have the same frequency, given by Eq. (3).

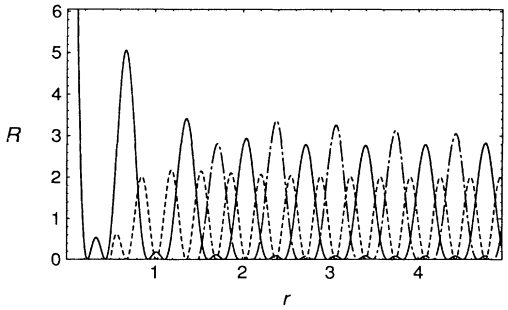


FIG. 8. Impedance ratio $R = R_3/R_1$ versus $r$: the solid line is for $s_0$, dashed for $a$, and dash-dotted for the $s_1$ mode.

### C. Many identical discontinuities

In the case of $N$ identical equidistant enlargements one should put $y_i = y$, $i = 1, 2, \ldots, N$, and $g_{i,i+1} = g$, $i = 1, 2, \ldots, N-1$, in Eq. (16). The resulting equation has the following properties.

It can be factorized in the form

$$(1-y)^{N-2} P_n(y) P_m(y) = 0 , \tag{25}$$

where $n, m$ are integers satisfying $n + m = N$ so that

$$n = \begin{cases} m & \text{for } N = 2m \\ m+1 & \text{for } N = 2m+1 , \end{cases}$$

and $P_n(y), P_m(y)$ are polynomials in $y$ of the power $n$ and $m$, except for the exponential dependence on $u = 1/y$ in their coefficients; cf. Eqs. (19) and (23) above. Equation $P_n(y) = 0$ has up to $n$ positive solutions corresponding to symmetric trapped modes. The actual number of the roots depends on the distance $g$ between discontinuities. It can be proved by induction that for any $g$ there is at least one solution and it behaves like $y \simeq 1/N$ at small distances, i.e., $k \simeq Nk_1$, because $P_n(y) \to 1 - Ny$ when $g/l_1 \to 0$. This solution corresponds to the maximal symmetric trapped mode, without nodes, as discussed in Secs. III A and III B for $N = 2$ and $N = 3$. It always has the largest frequency shift, i.e., the lowest frequency between all the trapped modes.

Equation $P_m(y) = 0$ gives up to $m$ solutions corresponding to antisymmetric trapped modes. At large distances, when $g/l_1 \gg 1$, the asymptotics of $P_j(y)$, $j = n, m$, are $(1-y)^j$ and there are $N = n + m$ solutions of Eq. (25) which asymptotically tend to 1. The degenerated roots $y = 1$ due to the explicit factor in Eq. (25) are extraneous ones.

As follows from discussions in Secs. III A and III B the physical interpretation of the both extremal cases, at small and large spacings, is quite obvious. At small distances between discontinuities they work together as a single combined discontinuity with effective area $A = A_1 + A_2 + \cdots + A_N$, which gives the maximal symmetric trapped mode with $k \simeq Nk_1$ for identical discontinuities. At large separations, the discontinuities do not feel each other and there exist $N$ independent trapped modes, each

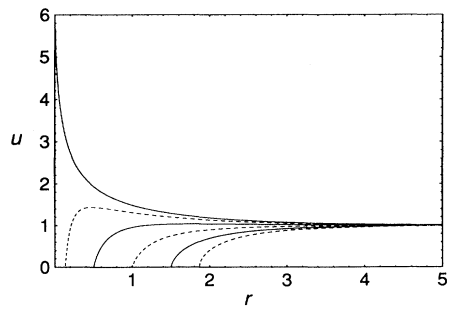


FIG. 9. Ratio $u = k/k_1$ versus $r$ for $N = 6$ identical discontinuities. Solid lines are for symmetric modes, dashed lines for antisymmetric modes.

localized around one of the discontinuities. These modes can be described by the equations of Sec. II for a single discontinuity.

Pictures of subsections $N = 2$ and $N = 3$ give some impression about frequencies and impedances of trapped modes for these particular cases. In addition, Fig. 9 gives an illustration of the solutions to Eq. (25) in the case of $N = 6$. There are three symmetric and three antisymmetric trapped modes.

## IV. MANY DISCONTINUITIES: PERIODIC STRUCTURES

### A. One discontinuity per period

In this section periodic arrays of discontinuities are considered. We assume that the period of the structure $D$ is longer than the waveguide diameter, $D > 2b$, and look for a solution of the Maxwell equations with frequency $\Omega$ below the waveguide cutoff, $\Omega < \omega_1$. According to Floquet's theorem, for periodic structures solutions must get a phase advance $\phi$ when the argument increases by one period, $f(z + D) = \exp(i\phi)f(z)$. As before, we restrict our consideration to only TM-type solutions with radial behavior given by Eq. (1), taking into account, however, that the same way of reasoning works for TE modes. Let us consider one period $-D/2 < z < D/2$ with an enlargement located at $z = 0$. Similar to Eq. (10) and using the same notations, one can write the $z$ dependence of the solution as

$$a\exp(kz) + b_{-1}\exp(-kz) \qquad \text{for} \quad -D/2 < z < 0\ ,$$

$$b\exp(-kz) + a_1\exp(kz) \qquad \text{for} \quad 0 < z < D/2, \quad (26)$$

where amplitudes $a, b$ correspond to the waves originated from the enlargement at $z = 0$, the wave with amplitude $b_{-1}$ comes from the previous period of the structure with the center at $z = -D$, and the wave with amplitude $a_1$ comes from the next period, with the center at $z = D$. From periodicity it follows that

$$b_{-1} = b\exp(-i\phi - kD) \qquad a_1 = a\exp(i\phi - kD)\ . \quad (27)$$

To find the frequency of the trapped mode we use continuity conditions and the reciprocity. The continuity at $z = 0$ requires $a + b_{-1} = b + a_1$. Taking into account relations (27), we apply the reciprocity theorem for the trapped mode under consideration and a regular waveguide TM mode with the same frequency $\Omega$ to get a simple equation for propagation constant $k$ for a given phase advance $0 \le \phi \le \pi$:

$$y - 1 - \exp(-kD)[(y + 1)\exp(-kD) - 2\cos\phi] = 0\ , \quad (28)$$

where, as well as in previous sections, $y = d/(kb)$ with $d = \mu_1^2 A/b^2 \ll 1$. Using new variables $u = 1/y = k/k_1$ and $p = dD/b = D/l_1$, one can rewrite it as

$$u = \frac{1 - e^{-2up}}{1 - 2e^{-up}\cos\phi + e^{-2up}} = \frac{\sinh up}{\cosh up - \cos\phi}\ . \quad (29)$$

Figure 10 shows solutions $u(p)$ for a few different values of parameter $\phi$. The value $\phi = 0$ corresponds to the solution with the period $D$ equal to that of the structure (the upper curve). It is the maximal symmetric mode, which has the largest frequency shift among all solutions, i.e., the lowest frequency. The lowest curve in Fig. 10 corresponds to $\phi = \pi$ and this is the antisymmetric mode with period $2D$, twice the structure period. In general, for an infinite periodic structure there is a continuum of solution to Eq. (29) for $0 < \phi < \pi$ which fills the whole range between these two extreme curves in Fig. 10. However, if the physical period consists of a finite number $M$ of discontinuities, like an accelerator ring with $M$ periods, the phase advance $\phi$ can only take discrete values $\phi_m = \pi m/M$, $m = 0, 1, \ldots M$, and there is a discrete set of up to $M + 1$ different solutions of Eq. (29). Three intermediate curves shown in Fig. 10 for the case $M = 4$ correspond (top to bottom) to $\phi = \pi/4$, $\pi/2$, and $3\pi/4$.

For a given $\phi > 0$, there is always the trivial solution $u = 0$ of Eq. (29) for every $p > 0$, and starting from some threshold value, there is also a positive solution $u(p) > 0$. For example, for $\phi = \pi$ this threshold value is $p = 2$. An interesting feature distinguishes the maximal symmetric mode $\phi = 0$ from other ones: there is no trivial solution in this case and there is no threshold since a positive solution $u(p) > 1$ exists for any positive value of $p$. It is clear from Fig. 10 that only for large distances between discontinuities ($p > 2$) there is a passband separated from the wavequide cutoff. When discontinuities are further separated, the width of this passband shrinks exponentially to the frequency of the trapped mode for a single discontinuity (cf. Sec. II) because $u(p) \simeq 1 + 2\cos\phi\exp(-p)$ for $p \gg 1$.

A simple study shows that solutions $u(p)$ for $\pi/2 \le \phi \le \pi$ monotonically increase from 0 staying less than 1 with $p$ increasing. Solutions for $0 < \phi < \pi/2$ have maximum $u(p^*) = 1/\sin\phi$ at $p^*$ given by $\cosh(p^*/\sin\phi) = 1/\cos\phi$. The maximal symmetric solution $u(p)$, which corresponds to $\phi = 0$, is monotonic and has no upper limit; its asymptotic for short periods is

$$u(p) \simeq \sqrt{2/p} = \sqrt{2l_1/D} \quad \text{for} \quad p \ll 1\ . \quad (30)$$

This behavior is quite different from that of the asymp-

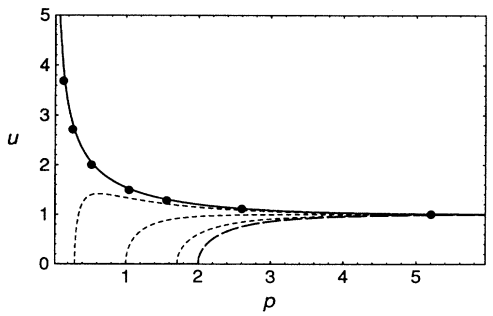


FIG. 10. Ratio $u = k/k_1$ versus $p = D/l_1$ for periodic structures. Thick points show numerical results.

totics in the case of a finite number of discontinuities, when $u$ tends to a finite limit (Sec. III). Since $u = l_1/l$, where $l_1 \equiv 1/k_1$ has the meaning of the length of the region occupied by the trapped mode for a single discontinuity [cf. Eq. (2)] and $l \equiv 1/k$, it gives a new "effective" length of the symmetric trapped mode in a periodic structure

$$l \simeq \sqrt{\frac{Dl_1}{2}} = \frac{b}{\mu_1}\sqrt{\frac{Db}{2A}} \ . \tag{31}$$

The frequency shift down from the cutoff frequency for this trapped mode becomes

$$\Delta\omega = \omega_1 \frac{\mu_1^2}{2}\left(\frac{Au}{b^2}\right)^2 = \omega_1 \frac{A}{bD} \ . \tag{32}$$

This simple answer has also a simple physical explanation. For a closed cylindrical cavity resonator of length $D$ and radius $b$ with a small axisymmetric enlargement, having area $A$ in the longitudinal cross section, on its side surface, the eigenfrequency of a given TM mode $\omega_0$ shifts down due to the enlargement present, e.g. [11],

$$\frac{\Delta\omega}{\omega_0} = \frac{1}{2}\frac{\int_{\Delta V} dV(|H|^2 - |E|^2)}{\int_V dV|H|^2} \propto \frac{A}{bD} \ , \tag{33}$$

where $E, H$ are the fields in the resonator without enlargement, $\Delta V$ and $V$ are volumes of the enlargement and cavity. In the transition to the expression (33), in the RHS it is taken into account that $|E| \ll |H|$ near the cavity wall. So, the relative frequency shift is proportional to the ratio of the volumes of the enlargement and cavity, as in Eq. (32).

One can imagine metallic transverse end planes in the middle between every two discontinuities in a periodic structure so that it transforms into a chain of adjacent identical cavities. Such walls do not change the fields and frequencies of the maximal symmetric trapped mode in the waveguide, which has a period equal to that of the structure. However, the analogy between Eqs. (32) and (33) works only when the fields fill the whole cavity, from one end wall to the other. It is exactly the case of trapped modes in short-period structures when $D \ll l_1$. One the other hand, for long periods ($D \gg l_1$) the argument of a closed cavity fails since the fields in a trapped mode do not reach the end walls, which is why the frequency shift is independent of the length of resonators.

It is appropriate to mention that starting from the well-known relation (33) one can easily derive qualitatively the frequency shift of the trapped mode for a single discontinuity Eq. (2). Indeed, if the mode frequency is given by Eq. (33), its propagation constant is

$$k \simeq \sqrt{2\omega_0\Delta\omega}/c = \mu_1/b\sqrt{2A/(bD)}$$

and the length of the mode propagation

$$l = 1/k = b/\mu_1\sqrt{bD/(2A)} \ .$$

These relations work until $l > D/2$, otherwise fields tear off the end surfaces of the resonator. One can estimate the resonator length when it occurs by putting $D = 2l$ in the equation above. If $D$ becomes larger, the mode frequency does not change any more because the fields do not reach the end walls. It gives

$$l = b^3/(\mu_1^2 A) \ ,$$

which is exactly the same as what follows from Eq. (2). Of course, the coincidence of the numerical factors is just by accident.

It is clear from the discussion above that one can check Eq. (32) by numerical computations using SUPERFISH [10] even more easily than in previous sections when one had to use very long resonators in order to avoid the influence of the end walls. The results of our numerical calculations for various resonator lengths (i.e., various periods) are shown in Fig. 10 and coincide well with the results from Eq. (29) with $\phi = 0$. Figure 11 shows fields of the lowest trapped mode calculated by the code for two periodic structures.

We restrict ourselves by calculating the resonant coupling impedance only for the lowest (maximal symmetric) trapped mode, since one can expect from considerations above that it gives the largest contribution. The impedance per period produced by this trapped mode can be calculated in the same way as above [cf. Eq. (20)], except the integration over $z$ should be limited to one period. The result is

$$R_p = R_1 \frac{\left(1 + e^{-up} + 2\frac{\mu_1}{d}e^{-up/2}\sin\frac{\mu_1 p}{2d}\right)^2}{1 + 2upe^{-up} - e - 2up} \ , \tag{34}$$

where $u = u(p)$ is a solution of Eq. (29) with $\phi = 0$ and $R_1$ is given by (6). The asymptotics of the impedance are: for large distances ($p \gg 1$), $R_p \to R_1$, i.e., to the impedance of a single discontinuity; for short distances where $2d \le p \ll 1$, i.e., $2b \le D \ll l_1 = b^3/(\mu_1^2 A)$,

$$R_p \to R_1 \frac{\{d + \sin[\mu_1 D/(2b)]\}^2}{d^{5/2}\sqrt{2D/b}} = \frac{Z_0}{\pi\delta}\sqrt{\frac{Ab}{2D}}\left(\sin\frac{\mu_1 D}{2b} + \frac{\mu_1 A}{b^2}\right)^2 \ .$$

An interesting feature of this last expression is that it behaves as $\sqrt{A}$, while in the opposite extreme $R_p \to R_1 \propto A^3$. Since $A$ is considered to be small ($d = \mu_1^2 A/b^2 \ll 1$), the impedance per period is much larger for short-period structures. It is illustrated by Fig. 12, which shows the

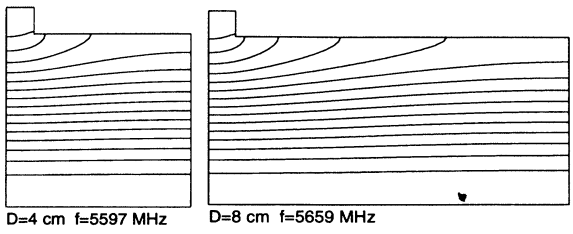


FIG. 11. Electric field lines in trapped modes for two periodic structures with different periods.

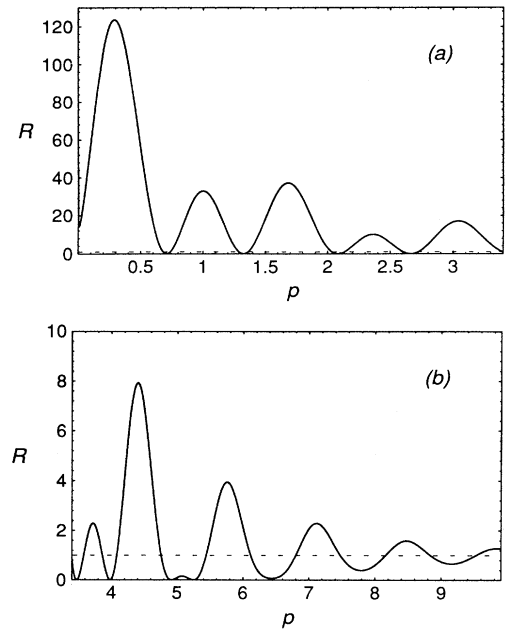


FIG. 12. Impedance ratio $R = R_p/R_1$ versus $p$ for periodic structures with a single discontinuity per period ($d = 0.26$). (a) and (b) have different scales.

impedance per period versus the period length.

It is worthwhile to relate $R_p$, calculated above, to the impedance of a cyclic accelerator. Let the accelerator vacuum chamber consist of a large number $M$ of periods of length $D$ and consider the lowest trapped mode in this structure, as described above. Calculating the coupling impedance of the ring according to Eq. (20) with $z$ integration over the whole ring and taking into account field periodicity, we get an extra interference factor to the impedance $R_p$ per period, Eq. (34), namely

$$R_M = R_p \frac{1}{M} \left( \frac{\sin(KMD/2)}{\sin(KD/2)} \right)^2 , \tag{35}$$

where $K = \Omega/c$ is the longitudinal wave number for a current harmonic with frequency $\Omega$ equal to that of the trapped mode.

One can easily realize that the interference factor in Eq. (35) has sharp maxima $M$ when $KD = 2m\pi$, $m = 1, 2, \ldots$, which leads to high impedance values, while for other $KD$ it is rather small. Since the value of $K$ is almost fixed by the chamber radius $K \simeq \mu_1/b$, one should avoid placing holes with period $D \simeq 2m\pi b/\mu_1$, choosing instead $D \simeq (2m+1)\pi b/\mu_1$, which makes $R_M \leq R_p/M$ due to destructive interference of trapped modes in adjacent periods of the structure. The physical meaning of the interference condition $KD = 2m\pi$ is obvious. It means that the number of the current wavelength $\Lambda = 2\pi/K$ on one period of the structure is an integer, $D = m\Lambda$, so that all periods work in phase.

The important quantity entering the stability conditions in circular accelerators, e.g., [2], is the so-called reduced longitudinal impedance $Z/n$, where $Z$ is the total impedance of the ring at given frequency $\omega$ and $n = \omega/\omega_{\rm rev}$ is the corresponding harmonic number of the revolution frequency $\omega_{\rm rev} = c/R$, with $R$ being the machine radius. The real part of the reduced coupling impedance of the ring is now

$$\frac{\mathrm{Re}\, Z}{n} = \frac{R_M}{n} = \frac{2\pi R_M}{KMD} = R_p \frac{\pi KD}{2} \left( \frac{\sin(KMD/2)}{(KMD/2)\sin(KD/2)} \right)^2 . \tag{36}$$

In the worst case of $KD = 2m\pi$, it transforms into

$$\frac{\mathrm{Re}\, Z}{n} = \frac{R_p}{m} ,$$

which means that the impedance per period $R_p$ given by Eq. (34) imposes the upper limit on the reduced impedance of the ring.

### B. A few discontinuities per period

Let us consider briefly the case when there is more than one enlargement per period of a periodic structure. Once again we introduce unknown amplitudes of a piecewise solution and apply restrictions from continuity, periodicity, and reciprocity to obtain a linear system of equations for the amplitudes. For the case of $N$ enlargements, there are $2N+1$ variables ($2N$ amplitudes and one propagation constant $k$) and $2N$ homogeneous equations. In fact, they differ from Eqs. (12) and (13) only by two first and two last equations (for the first and last enlargement), due to periodicity. The requirement of the determinant of the matrix $M_{2N}(k)$ on the LHS of the linear system to vanish gives an equation to solve for $k$. We restrict ourselves only by an example of the lowest mode ($\phi = 0$; cf. Sec. IV A) for $N = 2$, in which case this equation takes the form

$$\begin{aligned} &\det M_2(k)/[(1-y_1)(1-y_2)] \\ &= (1-y_1)(1-y_2) - e^{-2kg} y_1 y_2 - 2e^{-kD} \\ &\quad + e^{-2kD}(1+y_1)(1+y_2) - e^{-2k(D-g)} y_1 y_2 = 0 , \end{aligned} \tag{37}$$

where $D$ is the structure period, $g$ is the distance between the discontinuities, $g \leq D$, and $y_n$ are defined after Eq. (13). For long periods, $kD \gg 1$, Eq. (37) becomes just Eq. (14). For short distances $g$, when $kg \ll 1$, Eq. (37) is the same as Eq. (28) for one enlargement per period, but with $y = y_1 + y_2$, i.e., we have a single combined discontinuity.

When two discontinuities are identical, $y_1 = y_2 = y$, Eq. (37) transforms into a product of two (for either upper or lower sign) equations ($u = 1/y$):

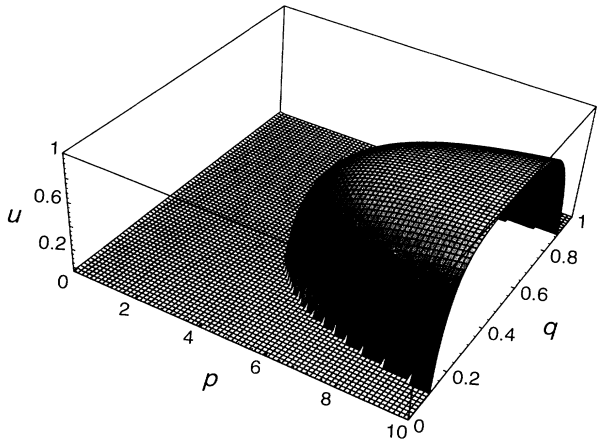


FIG. 13. Ratio $u = k/k_1$ versus $p = D/l_1$ and $q = g/D$ for periodic structures with two discontinuities per period, for the antisymmetric mode.

$$u = \frac{\cosh up/2 \pm \cosh u(p/2 - r)}{\sinh up/2} , \qquad (38)$$

where $p = dD/b$ and $r = dg/b$, $r \leq p$. In the particular case $D = 2g$, the first of these equations (upper sign) transforms into Eq. (29) with $\phi = 0$ and $p$ replaced by $r$, which corresponds to the maximal symmetric mode in the structure with period $g$ and one discontinuity per period. The second equation in the same particular case gives Eq. (29) with $\phi = \pi$ and $p$ replaced by $r$, and can be recognized as corresponding to an antisymmetric trapped mode, which has a period twice as long, $2g$. In the general case of arbitrary $p$ and $r$, this solution exists when (i) $p$ is large enough and (ii) both $q = r/p = g/D$ and $(1-q)$ are not very small. This statement is illustrated by Fig. 13, where the solution $u_a(p,r)$ of Eq. (38) for the lower sign is plotted as the function of $p$ and $q$. The same plot for the solution $u_s(p,r)$ of Eq. (38) with the upper sign is shown in Fig. 14. One can see that the frequency shift for the antisymmetric mode is always smaller than that for a single discontinuity ($u = 1$), while for symmetric solutions it is always larger. One can note that the cross section of surfaces in Figs. 13 and 14 by the plane $q = 1/2$ would reproduce two curves (the lowest and the upper ones) in Fig. 10 with $p$ replaced by $2p$.

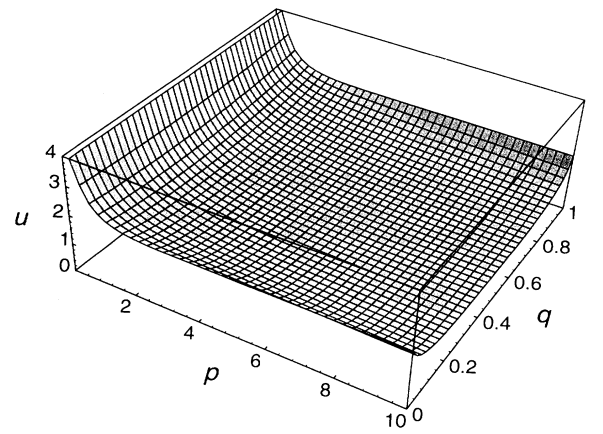


FIG. 14. Same as Fig. 13, but for the symmetric mode.

## V. EFFECTS OF TRAPPED MODES IN LINERS

It should be recalled that the results above are applicable to vacuum chambers not only with small enlargements but also with small pumping holes. The only difference is that for holes one should replace area $A$ of the enlargement cross section in all formulas by an "effective" area, as mentioned in Sec. II. For example, if there are $M$ holes in one transverse cross section of a cylindrical vacuum chamber, for an axisymmetric trapped mode, the following substitution takes place:

$$A \to \frac{\alpha_{\theta 1} + \alpha_{\theta 2} + \cdots + \alpha_{\theta M}}{4\pi b} , \qquad (39)$$

where $\alpha_{\theta_m}$, $m = 1, 2, \ldots, M$, denotes the magnetic susceptibility in the azimuthal direction of the $m$th hole in this transverse row and $b$ is the chamber radius. The sum occurs because all small pumping holes, having the same longitudinal position, contribute to the trapped mode additively, working as a single discontinuity. Holes at another longitudinal location work as another combined discontinuity. As follows from the results above, one can consider two small holes as having the same longitudinal position if their separation along the chamber axis is shorter than the chamber radius.

Bearing this in mind, we shall study trapped modes in a liner of a superconducting accelerator and give estimates of their contribution to the coupling impedance. As an example, we refer to the LHC vacuum chamber [5]. Its design anticipates the insertion of a special beam screen (liner) inside the cold (at 2 K) vacuum chamber of a circular cross section with an inner diameter of about 50 mm. The liner is a kind of inner pipe placed coaxially with the cold bore beam tube. It will be supported by thermal insulators and kept at a temperature 10–20 K by means of a separate helium cooling system, with cooling pipes in the coaxial space between the liner and the outer vacuum chamber. Such a beam screen has to prevent heating of the cold walls of the bore chamber and help to avoid vacuum problems due to photodesorption of residual gas molecules stuck to the cold wall. In the present design the liner has a square transverse cross section with rounded corners, rotated in such a way that diagonals of the square are in vertical and horizontal directions to provide the most space for the beam while fitting inside the bore pipe. The stainless-steel liner walls have thickness $t \simeq 1$ mm to resist distorting forces during magnet quenches and a thin (about 50 $\mu$m) copper coating of the inner wall surface to slow down the resistive wall instability. The inner distance between opposite plane walls of the liner is 35 mm.

To minimize the low-frequency coupling impedances, the pumping holes in the liner walls will have a shape of rounded-end narrow longitudinal slots with length $s = 6$ mm and width $w = 1.5$ mm. The total pumping

surface is 4% of the wall surface; this fraction was chosen from vacuum requirements. There are 666 pumping slots per meter of liner, with $M = 8$ slots in one transverse cross section, and the average longitudinal separation between adjacent cross sections with the slots (combined discontinuities) is $g = 1.2$ cm. The longitudinal periodicity of the slot distribution will be intentionally violated by displacing slots by small (a few millimeter) random distances along the chamber axis from their position in the periodic structure to avoid resonances due to periodicity which would otherwise occur at frequencies well above the cutoff, see Ref. [12]. Due to this randomized distribution the liner should not be treated as a periodic structure, especially with respect to the impedance estimate, but since discontinuities are very close, numerous and more or less evenly distributed, one can use results of Sec. IV to estimate the frequency shift of the lowest symmetric trapped mode and its interaction length. Taking into account that TM modes in a square, rounded-end waveguide are quite similar to those in a cylindrical one, we will take for estimates the "effective" chamber radius $b = 18$ mm. Then expression (39) takes the form

$$A \to \frac{M\alpha_\theta}{4\pi b} = \frac{Mw^2 s}{4\pi^2 b} , \tag{40}$$

where we use transverse magnetic susceptibility $\alpha_\theta = w^2 s/\pi$ for a narrow long slot in the thick wall, because $t \simeq w$; see, e.g., in [13,14]. As a result, the effective area to be substituted in formulas of Secs. III and IV is $A = 1.52 \times 10^{-3}$ cm$^2$. The length of the region which would be occupied by the field of the trapped mode for a single such discontinuity is $l_1 = b^3/(\mu_1^2 A) = 6.63$ m; cf. Eq. (2). Since this is much longer than the distance between adjacent discontinuities, they strongly interact each other, and because $g \ll l_1$, this situation is described by Eqs. (30)–(32) with $D = g = 1.2$ cm. It means that $u = \sqrt{2l_1/g} \simeq 33$ and the new effective length of the interaction $l = \sqrt{l_1 g/2} = 20$ cm. If we define the number of discontinuities that work as a single combined discontinuity by $N_{\rm eff} = 2l/g$, one can easily see that $N_{\rm eff} = u = 33$. The frequency shift for the trapped mode is given by Eq. (32):

$$\frac{\Delta\omega}{\omega_1} = 7 \times 10^{-4} ,$$

which is $\Delta f \simeq 5$ MHz for $f_1 \simeq 6.4$ GHz. The gap between the trapped mode frequency and the cutoff is rather small and one has to compare it with the width of the resonance due to energy dissipation in the walls and due to radiation from the slots: $\gamma = \gamma_1 + \gamma_{\rm rad}$. According to Eq. (4),

$$\frac{\gamma_1}{\omega_1} = \frac{\delta}{2b} \simeq \frac{2.3 \times 10^{-5}}{\sqrt{\mathcal{R}}} ,$$

where $\mathcal{R}$ is the ratio of the copper conductivities at cryogenic and room temperatures, which is usually 30–100. The radiation width for a thin wall would be [1]

$$\frac{\gamma_{\rm rad}}{\omega_1} \simeq N_{\rm eff} M \frac{\mu_1^3 k \alpha_\theta^2}{3b^5} \simeq 6 \times 10^{-5} .$$

However, for the thick wall, the external magnetic susceptibility $\alpha_{\rm ext} \simeq \exp[-\pi t/(2w)]\alpha_\theta$ should be used, which makes the radiation width much smaller, $\gamma_{\rm rad}/\omega_1 \simeq 7 \times 10^{-6}$. So the resonance width is small compared to the frequency gap and the trapped mode exists.

Let us proceed with impedance estimates. If discontinuities are far separated, $g > l_1$, the total impedance of the ring is just a sum of contributions (6) from all $N = 2\pi R/g$ discontinuities. Since $\omega \simeq \omega_1 = \mu_1 c/b$, it leads to the estimate

$$\frac{{\rm Re}\, Z}{n} = \frac{NR_1}{n} = \frac{2\pi b}{g\mu_1} R_1 = \frac{2Z_0 \mu_1^2 A^3}{\delta b^4 g} . \tag{41}$$

[In the case when $\gamma_{\rm rad}$ is not small compared to $\gamma_1$, in Eqs. (41) and (42) one should replace $2b/\delta$ by $\omega_1/\gamma$ with $\gamma = \gamma_1 + \gamma_{\rm rad}$.] However, the case of the LHC liner is different because $g \ll l_1$ and the interaction of discontinuities should be taken into account. One can consider each group of $N_{\rm eff}$ discontinuities (i.e., $N_{\rm eff}$ cross sections, each with eight slots) as a single combined one and the number of such group on the ring is $N_g = N/N_{\rm eff} = \pi R/l$. Then the estimate follows from Eq. (41) with replacements $N \to N/N_{\rm eff}$ and $R_1 \to N_{\rm eff}^3 R_1$ (cf. Sec. III):

$$\frac{{\rm Re}\, Z}{n} = N_{\rm eff}^2 \frac{2\pi b}{g\mu_1} R_1 = \frac{4Z_0 A^2}{\delta b g^2} , \tag{42}$$

which gives ${\rm Re}\, Z/n \simeq 165\ \Omega$ for the narrow-band impedance produced by the trapped modes in the LHC liner, if $\mathcal{R} = 100$. This value for the narrow-band coupling impedance is too large, even for such a high frequency.

In order to improve and generalize the impedance estimates above, one should consider that the pumping holes are not quite identical, they have some distribution of areas. It results in a frequency spread of resonances produced by different discontinuities. One can take account of the resonance overlapping using a weighted sum in calculating the total impedance of the ring, e.g. [15],

$$Z_{\rm tot}(\omega) = NZ(\omega) \to N \int dA w(A) Z(\omega, A) ,$$

where $w(A)$ is the area distribution, $\int dA w(A) = 1$, and $Z(\omega, A)$ is defined by Eq. (5). It is convenient to rewrite $Z(\omega, A)$ at frequencies near the resonance, i.e., when $\omega \simeq \Omega(A) = \omega_1 - \Delta\omega_1(A)$, as

$$Z(\omega, A) \simeq \frac{i\frac{\gamma}{\omega_1} R_1(A)}{1 - \frac{\omega_1}{\omega} + \frac{\Delta\omega_1(A)}{\omega} + i\frac{\gamma}{\omega}} ,$$

where $R_1(A)$ and $\Delta\omega_1(A)$ are the resonance impedance and frequency shift for the trapped mode caused by a discontinuity with area $A$. If the resonance width is small enough, namely, $\gamma \ll \Delta\omega_1(A) \ll \omega$, the integral over areas can be treated like a dispersion integral to get

$$\mathrm{Im} \int dA \frac{F(A)}{1 - \frac{\omega_1}{\omega} + \frac{\Delta\omega_1(A)}{\omega} + i\frac{\gamma}{\omega}} \simeq -i\pi \frac{F(A_*)}{\left| \frac{d}{dA} \frac{\Delta\omega_1(A_*)}{\omega} \right|} ,$$

where $A_* = A_*(\omega)$ is the solution to equation $\omega = \omega_1 - \Delta\omega_1(A_*)$.

In this way, we obtain two impedance estimates. For far separated discontinuities, i.e., $g \geq l_1$, the frequency shift is given by Eq. (3) and

$$\frac{\mathrm{Re}\, Z}{n} \simeq \pi Z_0 \frac{w(A)A^2}{bg} , \tag{43}$$

with $A$ being the averaged area per discontinuity. It should be noted that this estimate is applicable instead of Eq. (41) only when the *a posteriori* condition

$$\frac{\gamma}{\omega} < \frac{\mu_1^2 A}{\pi b^4 w(A)}$$

is valid. Otherwise, Eq. (43) would give higher value than (41), which is unacceptable because spreading of resonance frequencies due to the area distribution only reduces the impedance.

For interacting discontinuities $g \ll l_1$, the frequency shift is proportional to the area [cf. Eq. (32)], and the impedance estimate is

$$\frac{\mathrm{Re}\, Z}{n} \simeq 2\pi Z_0 \frac{w(A)A^2}{bg} . \tag{44}$$

Surprisingly, it is just twice the result of Eq. (43). For a specific distribution one should take $\max w(A)$ to get maximal impedance estimates (43) and (44). For example, for a Gaussian distribution of areas with standard deviation $\sigma_A$, it is $1/(\sqrt{2\pi}\sigma_A)$. If we assume $\sigma_A/A = 0.1$ and apply Eq. (44) for the LHC liner, it gives $\mathrm{Re}\, Z/n \simeq 7\ \Omega$. This estimate is lower than that from Eq. (42) and it is independent of the wall conductivity and radiation from slots.

It should be noted that an impedance estimate for a liner as a periodic structure, using Eqs. (34) and (36), would be much higher. However, the periodicity of pumping holes in the liner is violated by the very structure of the accelerator ring, which includes many irregularities such as interaction and utility regions, etc. An additional violation of the hole periodicity is introduced by randomization of the longitudinal distribution of slots in order to reduce high-frequency resonances; cf. [12]. Since even a small distortion of the periodicity drastically reduces the resonance coupling impedance of the structure (see [12,16]), the estimate (42) is more appropriate for the LHC liner case than if we would apply the impedance formulas of Sec. IV for periodic structures.

## VI. CONCLUSIONS

Trapped modes in waveguides with many small discontinuities such as enlargements or holes are studied both for periodic and nonperiodic structures. The existence conditions for trapped modes are considered and their frequencies are calculated. The calculated frequencies are in good agreement with results of numerical computations for particular cases. While our study concentrates on the lowest axisymmetric TM modes because of their importance for the beam-chamber coupling impedance calculations, the results can be easily applied for TE and higher-order modes, using propagation constants for these modes from [1] and formulas of Secs. III–V.

The magnitudes of the narrow-band resonances of the coupling impedance produced by the trapped modes are calculated. These results are applied to obtain coupling impedance estimates for the liners (thermal screens) of large superconducting colliders at frequencies near the cutoff. The practical conclusion for the liner design is to avoid an exact periodicity in the longitudinal distribution of the pumping holes and intentionally introduce some distribution of the hole areas (or slot lengths) to reduce effects of the trapped modes.

*Note added.* Very recent experimental studies of the beam pipes with many small holes [17] at CERN confirmed the existence of a few trapped modes with high $Q$ factors slightly below the $\mathrm{TE}_{11}$ mode cutoff frequency (the lowest one in a circular waveguide). The preliminary results of the frequency shift measurements for these trapped modes are in agreement with theory predictions within 10%.

## ACKNOWLEDGMENTS

The author would like to express his gratitude to Dr. V.I. Balbekov, Dr. R.L. Gluckstern, and Dr. G.V. Stupakov for useful discussions and remarks. This work was supported in part by the U.S. Department of Energy.

[1] G.V. Stupakov and S.S. Kurennoy, Phys. Rev. E **49**, 794 (1994).
[2] A.W. Chao, *Physics of Collective Beam Instabilities in High Energy Accelerators* (Wiley, New York, 1993).
[3] S. Heifets and S. Kheifets, Rev. Mod. Phys. **63**, 631 (1991).
[4] S.S. Kurennoy, Phys. Part. Nucl. **24**, 380 (1993).
[5] The LHC Study Group, CERN Report No. 91-03, 1991 (unpublished).
[6] R.L. Gluckstern (private communication).
[7] S. S. Kurennoy, Part. Accel. **39**, 1 (1992).
[8] G. V. Stupakov (private communication).
[9] R.E. Collin, *Field Theory of Guided Waves* (IEEE Press, New York, 1991).
[10] K. Halbach and R.F. Holsinger, Part. Accel. **7**, 213 (1976).
[11] L.A. Vainstein, *Electromagnetic Waves* (Radio i Svyaz', Moscow, 1988).
[12] S.S. Kurennoy, in *Proceedings of the 1993 Particle Accelerator Conference*, edited by S.T. Corneliussen (IEEE, Washington, DC, 1993), p. 3417.
[13] S.S. Kurennoy and G.V. Stupakov, Part. Accel. **45**, 95 (1994).
[14] S.S. Kurennoy, SSC Laboratory Report No. SSCL-636, 1993 (unpublished).
[15] V.I. Balbekov, Institute for High Energy Physics (Serpukhov) Report No. IHEP 93-55, 1993 (unpublished).
[16] V.I. Balbekov, Institute for High Energy Physics (Serpukhov) Report No. IHEP 85-128, 1985 (unpublished).
[17] F. Caspers and T. Scholz (private communication).